Residual nuclide production above 200 MeV

P. Armbruster[3)], J. Benlliure[2)], M. Bernas[1)], A. Boudard[4)], E. Casarejos[2)], S. Czajkowski[5)], T. Enqvist[6)], B. Jurado[1)], A. Kelić[3)] R. Legrain[4)], S. Leray[4)], B. Mustapha[1)], J. Pereira[2)], M. Pravikoff[5)], F. Rejmund[1)], M. V. Ricciardi[3)], K.-H. Schmidt[3)], C. Stéphan[1)], J. Taïeb[1)], L. Tassan-Got[1)], C. Volant[4)], W. Wlazło[4)]

[1)]IPN Orsay, IN2P3, F-91406 Orsay, France
[2)]University of Santiago de Compostela, E-15706 Santiago de Compostela, Spain
[3)]GSI, Planckstraße 1, D-64291 Darmstadt, Germany
[4)]DAPNIA/SPhN CEA/Saclay, F-91191 Gif sur Yvette, France
[5)]CENBG, IN2P3, F-33175 Gradignan, France
[6)]University of Jyväskylä, 40351 Jyväskylä, Finland

Contribution to the final HINDAS report

1. Introduction

While the nuclear reactions occurring in a conventional fission reactor are limited to the energy range of fission neutrons below a few MeV, the nuclear reactions occurring in an accelerator-driven system, consisting of a sub-critical reactor and a neutron source driven by 1 GeV protons extend to energies up to the primary proton energy. In addition to the detailed understanding of the neutronics and the complex transport phenomena of light particles, the production of heavy residues by proton- and neutron-induced fragmentation and fission reactions needs to be known for the design of such a system, because it has decisive consequences for the shielding and the activation of the installation, the radiation damages of construction materials and the chemical properties of the spallation target. In contrast to the situation in conventional fission reactors, where all relevant nuclear data could be measured, the large range of energy and the variety of target materials involved in an accelerator-driven system demands for a different strategy. Only a limited number of selected key reactions can be studied in full detail and serve to benchmark, improve and develop nuclear-reaction codes, which are then used to calculate the reactions occurring in the accelerator-driven system in their full variety.

2. Status before starting the HINDAS project

The conventional experiments on residual-nuclide production in proton- and neutron-induced reactions are performed by bombarding various target materials with protons or neutrons of the energy of interest and by analysing the produced species after irradiation, e.g. by their radioactive decay or by off-line and on-line mass spectrometry [ROS83, CUN47, WOL56, FRI63, KLA69, SAU83, GLO01]. These methods can only give a limited insight into the reaction mechanism, because short-lived products, which form the dominant production in most cases, cannot be observed due to the time delay between the irradiation and the measurement. Information on the reaction kinematics is also not easily accessible. In addition, stable nuclides could only be detected with much effort e.g. by off-line mass spectrometry. As documented in a comprehensive intercomparison [MIC97], the experimental information was insufficient to develop reliable models. In the course of the concerted action “Lead for ATD”, which preceded the HINDAS project, an innovative experimental method has been developed, which copes with this problem. This new approach is based on the bombardment of an hydrogen target with heavy projectiles. That means that the experiment is performed in inverse kinematics. The reaction products are identified in-flight in mass and atomic number in a high-resolution spectrometer. At the same time, information on the reaction kinematics is available. Using this technique, during the HINDAS project large sets of new experimental data with unprecedented quality have been accumulated.

Still, continued effort was invested using the conventional techniques, providing very important complementary information on the energy dependence of the production of specific nuclides. Such information, which is extremely valuable for the understanding of the energy dependence of the different reaction mechanisms, cannot easily be obtained by the inverse-kinematics technique due to the large effort for performing and analysing these experiments. In addition, the experiments based on decay spectroscopy give a direct measurement on long-term activation.

The combined information of these two techniques formed the basis for an improved understanding of the nuclear-reaction aspects and for essential improvements of the nuclear models, which now allow for performing considerably more realistic calculations.

3. Results on residual nuclide production and kinematics obtained in HINDAS

We report here on the complete isotopic production cross sections for a long series of elements, measured in the inverse-kinematics spallation reaction of 1 GeV protons and 2 GeV deuterons with

lead and uranium. In addition, the velocity distributions of all the produced isotopes were measured, giving crucial information on the reaction mechanisms involved. Most of these results have been published in scientific journals [WLA00, ENQ01, ENQ02, TAI03, BER03]. Others are documented in PhD theses [CAS01, PER03, RIC03] and will be published soon.

3.1. Experimental method

The experimental method and the analysis procedure have been developed and applied in previous experiments [JON98, ENQ99, BEN99, BEN01, REJ01]. The primary beam of 1 *A* GeV ^{208}Pb and 1 *A* GeV ^{238}U, respectively, was delivered by the heavy-ion synchrotron SIS at GSI, Darmstadt. The dedicated experimental set up is shown in Fig. 1. The proton target and the deuteron target were composed of 87.3 mg/cm^2 liquid hydrogen [CHE97] and of 206 mg/cm^2 liquid deuteron, respectively, enclosed between thin titanium foils of a total thickness of 36 mg/cm^2. The primary-beam intensity was continuously monitored by a beam-intensity monitor based on secondary-electron emission [JUN96, JUR02]. In order to subtract the contribution of the target windows from the measured reaction rate, measurements were repeated with the empty target. Heavy residues produced in the target were all strongly forward focused due to the inverse kinematics. They were identified using the Fragment Separator (FRS) [GEI92] and the associated detector equipment.

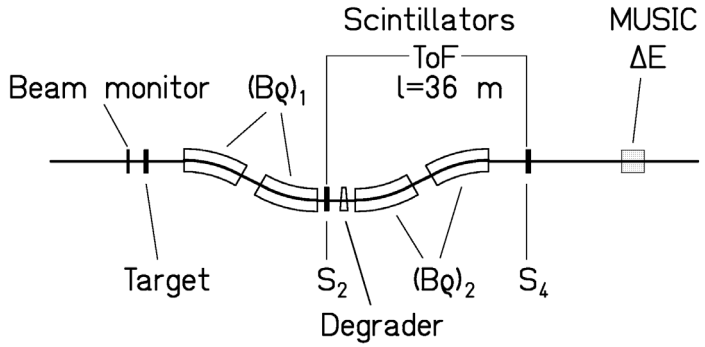

Figure 1: Schematic drawing of the fragment separator FRS with the detector equipment. For details see text.

The FRS is a two-stage magnetic spectrometer with a dispersive intermediate image plane (S_2) and an achromatic final image plane (S_4) with a momentum acceptance of 3% and an angular acceptance of about 15 mrad around the beam axis. Two position-sensitive plastic scintillators placed at S_2 and S_4, respectively, provided the magnetic- rigidity ($B\rho$) and time-of-flight measurements, which allowed determining the mass-over-charge ratio of the particles.

For an unambiguous isotopic identification of the reaction products, the analysis was restricted to ions, which passed both stages of the fragment separator fully stripped. The losses in counting rate due to the fraction of incompletely stripped ions and the losses due to secondary reactions in the layers of matter in the beam line were corrected for [ENQ01].

To identify all residues in the whole nuclear-charge range up to the projectile, it was necessary to use two independent methods in the analysis. The nuclear charges of the lighter elements, mainly produced by fission, were deduced from the energy loss in an ionisation chamber (MUSIC) with a resolution $Z/\Delta Z = 170$ obtained for the primary beam. Combining this information with the mass-over-charge ratio, a complete isotopic identification was performed. A mass resolution of $A/\Delta A = 480$ was achieved.

Since part of the heavier reaction products was not completely stripped, the MUSIC signal was not sufficient for an unambiguous *Z* identification. Therefore, the identification of reaction products of elements above terbium was performed with the help of an achromatic energy degrader [SCH87] placed at the intermediate image plane of the FRS. Degrader thicknesses of about 5 g/cm^2 of aluminium were used. The nuclear charge of the products was deduced from the reduction in magnetic rigidity by the slowing down in the energy degrader. The MUSIC signal was still essential for suppressing events of incompletely stripped ions and from nuclei destroyed by secondary

reactions in the degrader. The velocity of the identified residue was determined at S_2 from the $B\rho$ value and transformed into the frame of the beam in the middle of the target, taking into account the appropriate energy loss. More than 100 different values of the magnetic fields were used in steps of about 2 % in order to cover all the produced residues and to construct the full velocity distribution of each residue in one projectile-target combination.

The re-construction of the full velocity distribution allows for disentangling reaction products formed in fragmentation and fission reactions due to their different kinematic properties. The velocity distributions as a function of neutron number for 12 selected elements of one of the systems investigated are shown in Fig. 2 as cluster plots. It can be seen from the distributions that the reaction products can be attributed to different reaction mechanisms, i.e. spallation-evaporation and spallation-fission. For isotopes close to the projectile, one or two settings are able to cover the whole distribution of one isotope. Around mass region 150, three or four settings are needed. For isotopes produced by fission, only those emitted either in forward or in backward direction with respect to the primary beam can be observed in a given setting of the FRS because the angular acceptance is too small for sideward emitted fragments [BEN02]. The production of lighter elements from fragmentation ($Z \leq 60$, and mean velocity centred close to the primary-beam velocity) seen in Fig. 2, does not result from primary reactions in the liquid-hydrogen target, but from secondary reactions or from reactions in the titanium target windows.

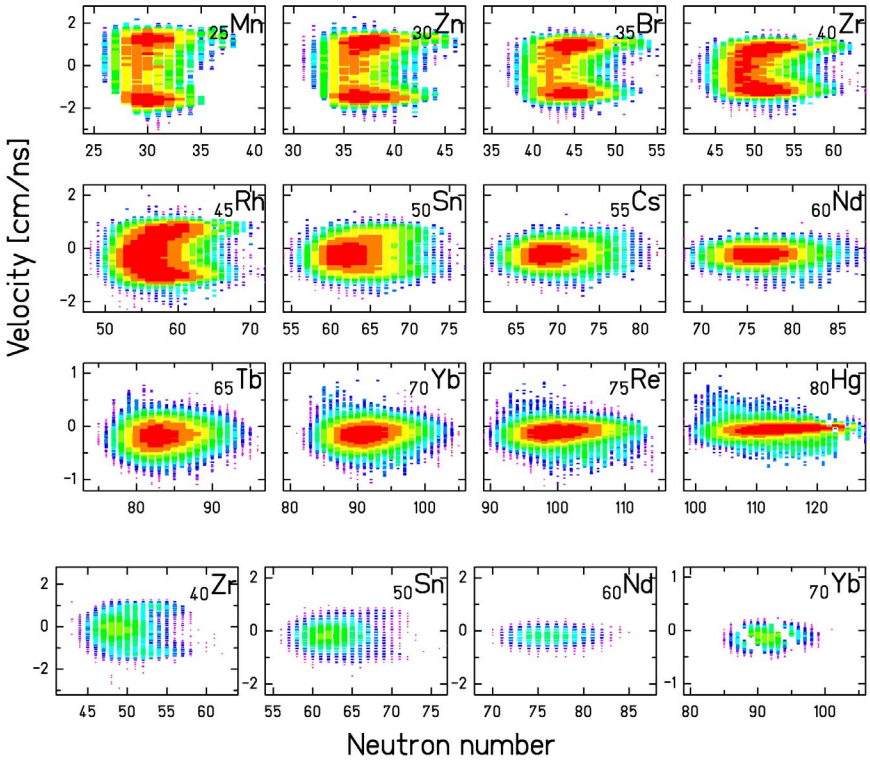

Figure 2: Two-dimensional cluster plots of velocity versus neutron number for 12 selected elements produced in the reaction ^{208}Pb + ^{2}H at 1 *A* GeV. The three uppermost rows show the reaction rate with the full target and the lowest row with the empty target (target windows). The velocity is given in the centre-of-mass system of the primary beam in the middle of the target. The intensity scale is logarithmic and different for each element, the full and empty target contributions can directly be compared. The distribution of the ytterbium isotopes produced in the empty target was incompletely measured, the contributions of the three spectrometer settings are visible. Note also the different scales in velocity in different rows.

3.2 Measured cross sections

The production of residual nuclides has been investigated for four systems which are particularly relevant for the design of accelerator-driven systems. The production rates were measured for a

total number of 1056 nuclides in the reaction ^{208}Pb + ^{1}H, for 1037 nuclides in the reaction ^{208}Pb + ^{2}H, for 1220 nuclides in the reaction ^{238}U + ^{1}H, and for 1369 nuclides in the reaction ^{238}U + ^{2}H. These data are depicted on a chart of the nuclides in Figs. 3 and 4. The velocity distributions of all these nuclides were determined at the same time. The different regions on the chart of the nuclides, produced by spallation-evaporation and by spallation-fission reactions, respectively, can clearly be distinguished. In the reactions with the deuteron target, which induce roughly a factor of two more energy into the system, the production of spallation-evaporation residues extends to appreciably lighter nuclides, while the fission distributions are much less affected. This can be also seen in Fig. 5, which compares the isotopic distributions for several elements measured in the reactions of ^{238}U in proton- and deuteron-target.

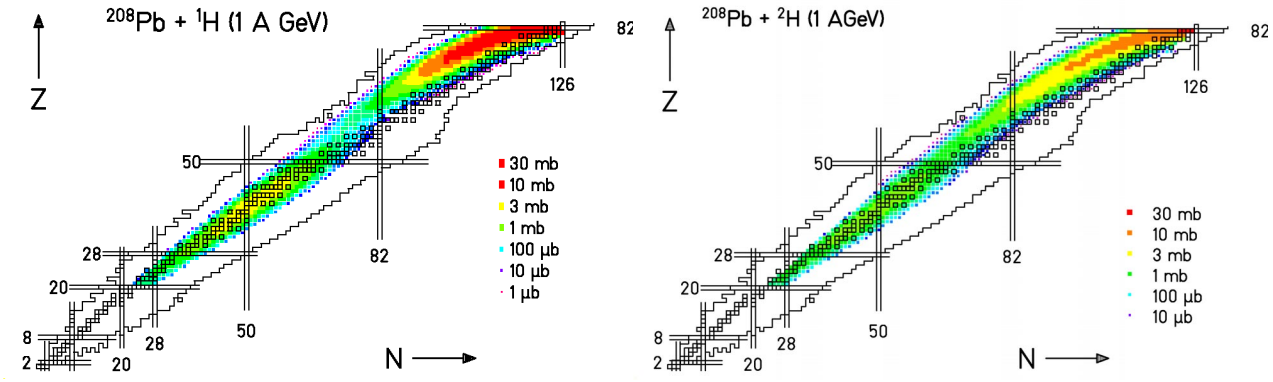

Figure 3: Residual nuclide cross sections for the reaction ^{208}Pb + ^{1}H and ^{208}Pb + ^{2}H at 1 *A* GeV on a chart of the nuclides. Primordial nuclei are marked by open squares, the outer line gives the range of known nuclides, and the shell closures are indicated by double lines.

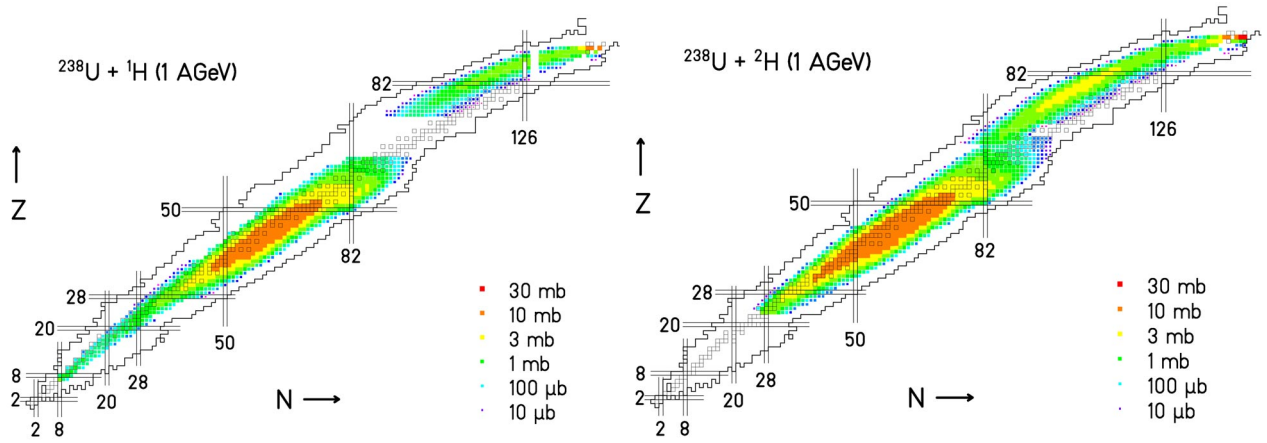

Figure 4: Residual nuclide cross sections for the reaction ^{228}U + ^{1}H and ^{238}U + ^{2}H at 1 *A* GeV.

For the elements close to the ^{238}U projectile, the production cross sections are almost the same. In fact, these isotopes are produced in very peripheral collisions, where in the case of the deuteron-induced reaction only one nucleon, i.e. the proton or the neutron, interacts with the projectile making then the reactions ^{238}U (1 *A* GeV) + p and ^{238}U(1 *A* GeV) + d looking similar. On the other hand, going away from the projectile (e.g. *Z*= 76, 80 in Figure 5) deviations between these two

reactions appear. This is a region, where both nucleons of the deuteron target interact with the projectile, thus introducing almost two times more excitation energy in the first stage of reaction compared to the proton-induced reaction. This would then results in not only higher cross sections for the production of light spallation-evaporation residues, but also in the production of lighter spallation-evaporation residues (see Fig. 4) in the reaction ^{238}U(1 *A* GeV) + d as compared to the reaction ^{238}U(1 *A* GeV) + p.

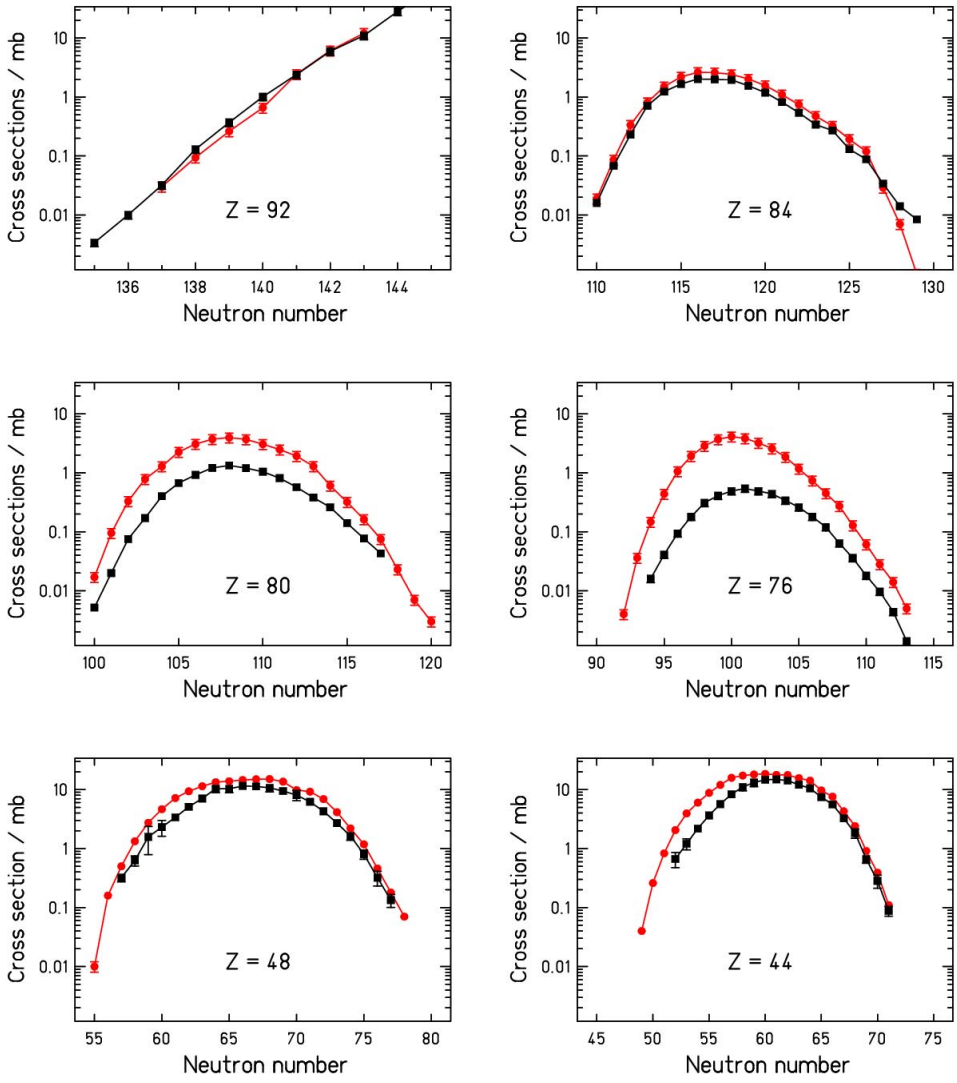

Figure 5: Isotopic distributions for several elements measured in the reactions of ^{238}U at 1 *A* GeV with protons (black squares) and deuterons (red dots).

In fission cross sections, there are not so many differences to be expected between these two reactions, as can be seen in Figures 4 and 5. In the case of lighter fission fragments (e.g. *Z*=44 in Fig. 5), the neutron-deficient isotopes are produced slightly more abundantly in the ^{238}U + d reaction, while the neutron-rich side seems to be equally populated. This difference can be understood as an indication that the prefragments from the reaction ^{238}U + d extend to higher excitation energies, and thus the evaporation chains extend to lighter and more neutron-deficient fission fragments. All this discussion is also valid for the ^{208}Pb + p,d reactions at 1 *A* GeV.

Another valuable information on the reaction aspects that these data can provide concerns the influence of dissipation on the fission dynamics at high excitation energies.

Thanks to the measurement of the full isotopic chains, we are able to produce sensible isobaric cross sections, this means, cross sections summed up over the full isobaric chains. The associated plot is reproduced in Fig. 6, which shows the isobaric distributions for three reactions: ^{238}U + p,

^{208}Pb + p, both at 1 *A* GeV, and ^{197}Au + p at 0.8 *A* GeV from Ref. [REJ01]. The isobaric cross section is figured as a function of the mass loss.

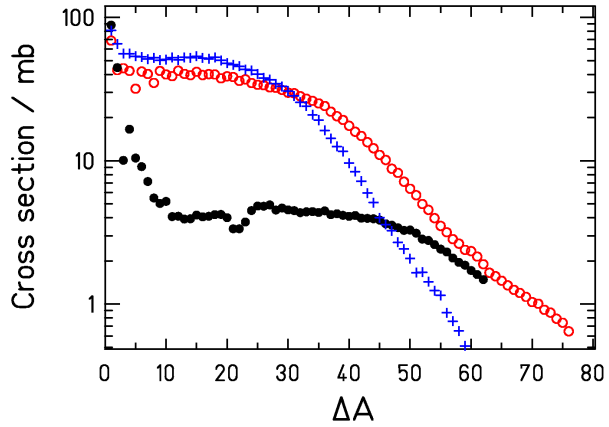

Figure 6: Isobaric cross sections as a function of mass loss for three reactions: The full symbols mark the system ^{238}U + ^{1}H at 1 *A* GeV, open symbols represent the system ^{208}Pb + ^{1}H at 1 *A* GeV, and the crosses result from the reaction ^{197}Au + ^{1}H at 0.8 *A* GeV [REJ01].

As far as low-fissility nuclei are concerned (gold and lead), the trends are very much similar. The main difference can be observed for the lowest mass. The lighter evaporation residues are less produced in the gold experiment. The explanation appears clearly when one considers the difference in term of projectile energy. Within the frame of a two-stage model, the first phase of the interaction leads to the production of an excited nucleus. The excitation spectrum depends on the energy of the projectile. The fastest projectile leads to the highest excitation energy (as far as the so-called limiting fragmentation regime is not reached) inducing the longest evaporation chain and producing the lightest evaporation residues. The height of both distributions (spallation of gold and lead) is similar for the heaviest residues. Concerning the spallation of uranium, the shape and the height of the isobaric distribution is pretty different.

As far as uranium is concerned, we notice a slight dip for mass losses close to 22. This depression is due to the very fast alpha decay of $N = 128$ isotones toward the 126-neutron shell. In fact, several isotopes characterized by a number of 128 neutrons decay by α emission toward the 126-neutron shell. The decay period of those isotopes is of the order of the time-of-flight through the FRS (~ 150 ns eigen-time). Therefore, part of the production is lost before being analysed and identified. Moreover, when the decay occurs at the very beginning of the flight path, the ion is ”seen” as the daughter nucleus. This effect causes the slight “hump” that can be observed. Below a loss of 60 mass units, the cross sections are notably lower in the uranium case than obtained for the two other experiments. The effect is stronger for the heaviest fragments. The explanation lies in the strong depletion effect of the fission process for actinide nuclei. During the evaporation phase, the fission probability is much higher for actinides than for rare earth nuclei, which are involved in spallation of gold or lead. Thus, in the case of uranium, the production of evaporation residues is paradoxically very much influenced by the fission mechanism.

Looking carefully at the isobaric cross sections shown in Fig. 6, the first qualitative observation is that the distributions associated to the lead and uranium experiments join for mass loss close to 60. The depletion effect observed on the cross section for the heaviest nuclei seems to vanish for the lightest evaporation residues. In the two-stage model, this observation seems surprising. Actually, the first step of the reaction leads to the production of an excited prefragment. The mass and nuclear charge of this nucleus is close to the one of the projectile (5 to 10 nucleons could be removed). Therefore, the light evaporation residues (for instance with a mass loss equal to 60 compared to the projectile) are consecutive to a very long evaporation chain starting in the actinide region. The fact that the light evaporation residues are not depopulated in the uranium case compared to the lead one indicates that the fission probability along the extensive de-excitation path

is rather low. This rather astonishes considering that this path crosses the actinide and pre-actinide regions, where the fission barriers are low. The explanation lies in the inhibition of the fission process for highly excited nuclei. In such a case, the typical de-excitation times are rather short, always much shorter than the time needed for equilibrating the fission-degree of freedom. Consequently, the fission channel is not open for highly excited actinides. When the nucleus cools down, emitting nucleons and light charged particles, the typical emission time increases, allowing the fission process to occur. For more details, see the Theory report of the High-Energy contribution.

3.3 Velocity distribution

The experimental set up allows determining the recoil-velocity properties of the produced nuclei. In this section, we present the results for the systems ^{238}U + p and ^{208}Pb + p. The values for the system ^{238}U + d and ^{208}Pb + d turned out to be rather similar.

For the spallation-evaporation residues, the velocity distributions are well represented by Gaussian distributions. The mean value and the standard deviation of the recoil-velocity distribution were determined for each ion. The slowing down in the target area, assuming that the nuclear reaction occurred in the middle of the target on the average, was accounted for.

In Figure 7a are plotted the mean velocities normalised following the prescriptions of Morrissey [MOR89] for systems ^{238}U + p and ^{208}Pb + p. Thus, we introduce $p'_{\|}$, which is the longitudinal recoil momentum, normalized in the following way:

$$p'_{\|} = v_{\|} * M_p * (\beta\gamma(\gamma+1))$$

This normalisation allows an inter-comparison of various measurements realised at different projectile energies. The location straggling is also unfolded for estimating the standard deviation of the velocity distribution. Note, however, that this contribution is negligible. Figure 7a also includes the empirical systematics stated by Morrissey [MOR89], which predicts a linear dependence between the reduced recoil momentum ($p'_{\|}$) and the mass loss (relative to the mass of the projectile). We observe that the systematics describes reasonably well the measured data. The width of the longitudinal recoil momentum acquired in the spallation-evaporation reaction is shown in Figure 7b for systems ^{238}U + p and ^{208}Pb + p. Again, the data are compared with the systematics of Morrissey, and also with the predictions of the Goldhaber model [GOL74]. While the systematics better represents the data for mass losses below $\Delta A = 20$, the experimental values increase more strongly for large mass losses and reach the prediction of the Goldhaber model for $\Delta A \approx 55$.

The mean velocity values induced in the fission process are shown in Fig. 8 for systems ^{238}U + p (left part) and ^{208}Pb + p (right part) both measured at 1 *A* GeV. The velocity values are obtained from the plots similar to Fig. 2, averaged over the mass and corrected for the effect of the finite angular acceptance of the FRS. All fission velocities are consistent with the binary decay of a heavy nuclear system between lead and uranium for the ^{238}U + p reaction, and between hafnium and lead in the case of the ^{208}Pb + p reaction. The strong variation of the fission velocity with the atomic number of the fission fragment is mostly given by momentum conservation.

4. Conclusion

A total number of 4682 individual nuclide production cross sections and velocity distributions in the reactions of 1 *A* GeV ^{238}U and ^{208}Pb with hydrogen and deuterium have been studied, covering most elements between oxygen and uranium. The reaction products were fully identified in atomic number *Z* and mass number *A* using the magnetic spectrometer FRS. Moreover, the velocity distribution of each individual nucleus was measured.

The data, production cross sections and energies, are of highest interest for the design of accelerator-driven systems. Using the measured production cross sections, combined with the

known decay properties, the short- and long-term radioactivities in the target material can be calculated. The number of atomic displacements being the reason for radiation damages in the structural materials can now be estimated from the measured kinetic-energy distributions. The data also allow estimating the admixtures of specific chemical elements in the liquid target, accumulated in long-term operation of the reactor, which enhance the corrosion of the walls or any material in the container.

The systems investigated provide stringent constraints to nuclear-reaction codes, in particular to the modelling of the fission competition and the nuclide production in fission. The new data will help to develop improved models with better predictive power for spallation reactions involving highly fissile nuclei.

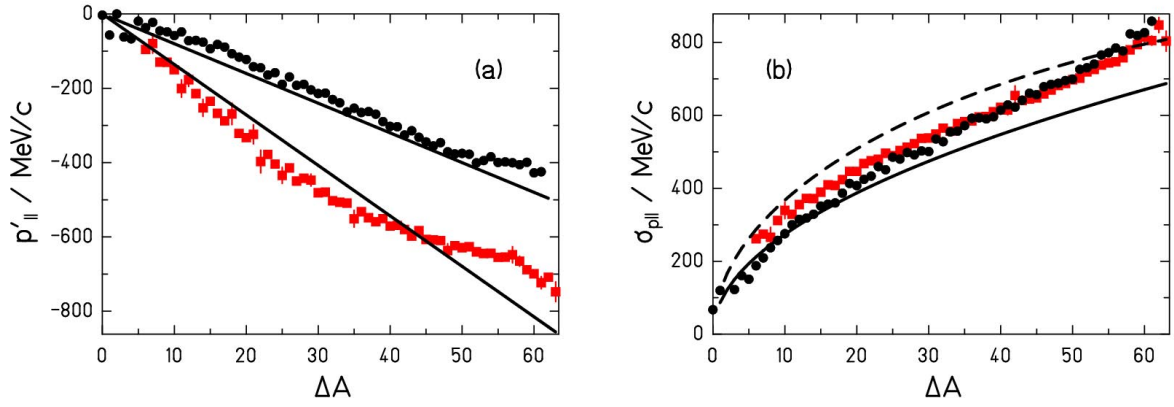

Figure 7: (a) Mean recoil momentum induced in the spallation of ^{238}U (black dots) and ^{208}Pb (red squares) by 1 GeV protons as a function of mass loss. The experimental data (symbols) are compared with the systematics of Morrissey [MOR89] (full line). (b) Standard deviation of the longitudinal momentum distribution of the spallation-evaporation residues produced in the bombardment of ^{238}U and ^{208}Pb with 1 GeV protons. The experimental data (symbols) are compared with the Goldhaber model [GOL74] (dashed line) and with the Morrissey systematics [MOR89] (full line). Since the measurement has been performed in inverse kinematics, the measured momenta and standard deviation are transformed into the frame of the beam.

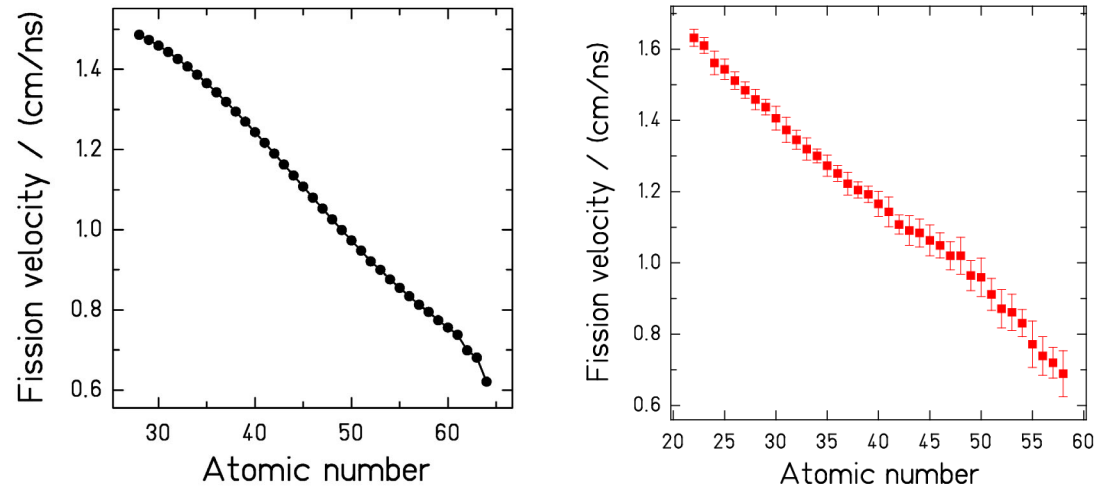

Figure 8: Measured mean velocities of the fission fragments produced in the spallation-fission reaction of ^{238}U (left) and ^{208}Pb (right) induced by 1 GeV protons as a function of the atomic number of the fission fragments. Since the measurement has been performed in inverse kinematics, the velocities are transformed into the frame of the beam.

References:

[BEN99] J. Benlliure *et al.* 1999, Production of neutron-rich isotopes by cold fragmentation in the reaction ^{197}Au + Be at 950 A MeV, *Nucl. Phys.* A 660 87-100.

[BEN01] J. Benlliure *et al.*, Isotopic production cross sections of fission residues in 197Au on proton collisions at 800 A MeV, *Nucl. Phys*. A 638 (2001) 513-539.

[BEN02] J. Benlliure, J. Pereira-Conca, K.-H. Schmidt, New approach to determine the angular transmission in zero-degree magnetic spectrometers, *Nucl. Instrum. Methods* A 478 (2002) 493-505.

[BER03] M. Bernas *et al.*, Fission residues produced in the spallation reaction 238U + p at 1 A GeV, *Nucl. Phys.* A 725 (2003) 213-253.

[CAS01] E. Casarejos, PhD thesis, 2001, University of Santiago de Compostela, Spain.

[CHE97] P. Chesny *et al.* 1997, Liquid hydrogen target for cross section measurements relevant for nuclear waste incineration, *GSI Scientific Rep. 1996, GSI 97-1,* 190.

[CUN47] B.B. Cunningham *et al.* 1947, *Phys. Rev.* 72 739.

[JON98] M. de Jong *et al*. 1998, Fragmentation cross sections of relativistic ^{208}Pb projectiles, *Nucl. Phys.* A 628 479-492.

[JUR02] B. Jurado, K.-H. Schmidt, K.-H. Behr, Application of a secondary-electron transmission monitor for high-precision measurements of relativistic heavy-ion beams, *Nucl. Instrum. Methods* A 483 (2002) 630.

[ENQ99] T. Enqvist *et al*. 1999, Systematic experimental survey on projectile fragmentation and fission induced in collisions of ^{238}U at 1 A GeV with lead, *Nucl. Phys.* A 658 47-66.

[ENQ01] T.Enqvist *et al*., Isotopic yields and kinetic energies of primary residues in 1 A GeV ^{208}Pb + p reactions, *Nucl. Phys.* A. 686 (2001) 481-524.

[ENQ02] T.Enqvist *et al*., Primary residue production cross sections and kinetic energies in 1 A GeV 208Pb on deuteron reactions, *Nucl. Phys.* A. 703 (2002) 435-465.

[FRI63] E.M. Friedlander *et al*. 1963, Excitation Functions and Nuclear Charge Dispersion in the Fission of Uranium by 0.1- to 6.2-GeV Protons, *Phys. Rev.* 129 1809-1825.

[GEI92] H. Geissel *et al*. 1992, The GSI projectile fragment separator (FRS) - a versatile magnetic system for relativistic heavy ions, *Nucl. Instrum. Methods* B 70 286-297.

[GLO01] M. Gloris *et al.* 2001, Proton-induced production of residual nuclei in lead at intermediate energies, *Nucl. Instr. Meth*. *Phys. Res*. A 463 (2001) 593-633.

[GOL74] A. S. Goldhaber, Statistical models of fragmentation processes, *Phys. Lett. B 53 (1974) 306-308.*

[JUN96] A.R. Junghans *et al.* 1996, A self-calibrating ionisation chamber for the precise intensity calibration of high-energy heavy-ion beam monitors, *Nucl. Instrum. Methods* A 370 312-314.

[KLA69] R. Klapisch, Mass Separation for Nuclear Reaction Studies, Ann. Rev. Nucl. Science 19 (1969) 33-60.

[MIC97] R. Michel, P. Nagel, 1997, *International Codes and Model Intercomparison for Intermediate Energy Activation Yields*, NSC/DOC(97)-1, NEA/OECD, Paris.

[MOR89] D.. Morrissey, Systematics of momentum distributions from reactions with relativistic ions, *Phys. Rev. C 39 (1989) 460-470.*

[PER03] J. Pereira, PhD thesis, 2003, University of Santiago de Compostela, Spain.

[REJ01] F. Rejmund *et al.*, Measurement of isotopic cross sections of spallation residues in 800 A MeV ^{197}Au + p collisions, *Nucl. Phys*. A 638 (2001) 540-565.

[RIC03] M. V. Ricciardi, PhD thesis, 2003, University of Santiago de Compostela, Spain.

[ROS83] G. Rossi, 1983, *Z. Phys.* 82 151.

[SAU83] H. Sauvageon, S. Regnier, G.N. Simonoff, 1983, Production of Kr and Xe isotopes by interaction of ^{197}Au with 0.15-0.24 GeV protons, *Z. Phys.* A 314 181-190.

[SCH87] K.-H. Schmidt *et al*., The momentum-loss achromat - a new method for the isotopical separation of relativistic heavy ions, 1987, *Nucl. Instrum. Methods* A 260 287-303.

[TAI03] J. Taieb *et al.*, Evaporation residues produced in the spallation reaction ^{238}U + p at 1 A GeV, *Nucl. Phys*. A 724 (2003) 413-430.

[WLA00] W. Wlazlo *et al*. 2000, Cross sections of spallation residues produced in 1 A GeV ^{208}Pb on proton reactions, *Phys. Rev. Lett.* 84 5736.

[WOL56] R. Wolfgang *et al*. 1956, Radiochemical studies of the interaction of lead with protons in the energy range 0.6 to 3.0 BeV, *Phys. Rev.* 103 394-403.